

# Interaction effects on galaxy pairs with Gemini/GMOS- I: Electron density

A. C. Krabbe<sup>1\*</sup>, D. A. Rosa<sup>1</sup>, O. L. Dors Jr.<sup>1</sup>, M. G. Pastoriza<sup>2</sup>, C. Winge<sup>3</sup>,  
G. F. Hägele<sup>4,5</sup>, M. V. Cardaci<sup>4,5</sup> and I. Rodrigues<sup>1</sup>

<sup>1</sup> Universidade do Vale do Paraíba, Av. Shishima Hifumi, 2911, Cep 12244-000, São José dos Campos, SP, Brazil

<sup>2</sup> Instituto de Física, Universidade Federal do Rio Grande do Sul, Av. Bento Gonçalves, 9500, Cep 91359-050, Porto Alegre, RS, Brazil

<sup>3</sup> Gemini Observatory, c/o AURA Inc., Casilla 603, La Serena, Chile

<sup>4</sup> Instituto de Astrofísica de La Plata (CONICET La Plata–UNLP), Argentina.

<sup>5</sup> Facultad de Ciencias Astronómicas y Geofísicas, Universidad Nacional de La Plata, Paseo del Bosque s/n, 1900 La Plata, Argentina

Accepted -. Received -.

## ABSTRACT

We present an observational study about the impacts of the interactions in the electron density of H II regions located in 7 systems of interacting galaxies. The data consist of long-slit spectra in the range 4400–7300 Å, obtained with the Gemini Multi-Object Spectrograph at Gemini South (GMOS). The electron density was determined using the ratio of emission lines  $[\text{S II}]\lambda 6716/\lambda 6731$ . Our results indicate that the electron density estimates obtained of H II regions from our sample of interacting galaxies are systematically higher than those derived for isolated galaxies. The mean electron density values of interacting galaxies are in the range of  $N_e = 24 - 532 \text{ cm}^{-3}$ , while those obtained for isolated galaxies are in the range of  $N_e = 40 - 137 \text{ cm}^{-3}$ . Comparing the observed emission lines with predictions of photoionization models, we verified that almost all the H II regions of the galaxies AM 1054A, AM 2058B, and AM 2306B, have emission lines excited by shock gas. For the remaining galaxies, only few H II regions has emission lines excited by shocks, such as in AM 2322B (1 point), and AM 2322A (4 points). No correlation is obtained between the presence of shocks and electron densities. Indeed, the highest electron density values found in our sample do not belong to the objects with gas shock excitation. We emphasize the importance of considering these quantities especially when the metallicity is derived for these types of systems.

**Key words:** galaxies: ISM

## 1 INTRODUCTION

The study of physical processes involved in galaxy collisions and mergers in the local universe is fundamental to understand the formation and evolution of these objects, providing important constraints in simulations of the universe at large scale.

In particular, the chemical abundance is highly modified in interacting/merging galaxies. Kewley et al. (2010) presented a systematic investigation about metallicity gradients in close pairs of galaxies. These authors determined the oxygen abundance (generally used as a tracer of the metallicity  $Z$ ) along the disk of eight galaxies in close pairs and found metallicity gradients shallower than the ones in isolated galaxies. Similar results have been reached by Krabbe et al.

(2011, 2008), who built spatial profiles of oxygen abundance of the gaseous phase of the galaxy pairs AM 2306-721 and AM 2322-2821. This flattening in the oxygen abundance gradient reflects the effects of gas redistribution along the galaxy disk due to metal-poor inflow of gas from outskirts of the centre of interacting galaxies (Rupke et al. 2010).

The large-scale gas motion created by the interaction induces high star formation rate and galactic-scale outflows (Veilleux et al. 2005), producing shock excitation in star-forming regions, such as reported in recent studies of Luminous Infrared Galaxies by Soto & Martin (2012) and Rich et al. (2012, 2011). In particular, Rich et al. (2011), through integral field spectroscopic data of the Luminous Infrared Galaxies IC 1623 and NGC 3256, showed that broad line profiles are often associated with gas shock excitation in H II regions located in mergers. Similar results were also found by Newman et al. (2012) for the clumpy star-forming

\* E-mail:angela.krabbe@gmail.com

galaxy ZC 406690 (see also Soto et al. 2012). These authors pointed out that the broad emission likely originates from large-scale outflows with high mass rates from individual star-forming regions. The changes in galaxies that experience an encounter seem to have a relation with the separation among the objects interacting, such as showed by Scudder et al. (2012). These authors, using spectroscopy data of a large sample of objects with a close companion taken from Sloan Digital Sky Survey Data Release, found that the metallicity gradient and the star formation rate (SFR) are correlated with the separation of the galaxy pairs analysed, in the sense that the gradients are flatter and the SFR are higher at smaller separations.

Despite recent efforts to probe the properties of interacting galaxies, the electron density of star-forming regions have been poorly determined in these systems, as well as its correlation with other quantities (e.g.  $Z$ , SFR). In galaxy disks of interacting galaxies, where gas motions and gas excited by shock are present, high electron density is expected and, can be used as a signature of the presence of these motions and shocks. In fact, Puech et al. (2006), in a study about galaxy interaction, mapped electron densities in six distant galaxies ( $z \sim 0.55$ ) and found that the highest electron density values observed could be associated to the collision between molecular clouds of the interstellar medium and gas inflow/outflow events. These authors derived electron density values lower than  $400 \text{ cm}^{-3}$ , typical of classical H II regions (Copetti et al. 2000; Castañeda et al. 1992). However, Puech et al. (2006) used as a sensor the  $[\text{O II}]\lambda 3729/\lambda 3727$  ratio, which underestimates the electron density in relation to determinations via other line ratios (Copetti & Writzl 2002). Most of oxygen determinations of the gas phase in interacting galaxies (e.g. Scudder et al. 2012; Rich et al. 2012, 2011; Krabbe et al. 2011; Kewley et al. 2010; Krabbe et al. 2008) are based on theoretical models that consider low electron density values of  $10\text{-}200 \text{ cm}^{-3}$  (Krabbe et al. 2011; Dors et al. 2011; Kewley & Dopita 2002; Dopita et al. 2000). If the electron density values considerably differ of those considered in the models, the oxygen abundance estimations will be doubtful. In fact, Oey & Kennicutt (1993) showed that systematic variations in the nebular density introduce significant uncertainties into the abundances obtained using methods based on strong emission lines. They found that differences between  $10$  and  $200 \text{ cm}^{-3}$ , a typical range for the electron density derived in giant H II regions (e.g. Copetti et al. 2000; Castañeda et al. 1992; Kennicutt 1984; O'dell & Castañeda 1984), reflect variations up to  $0.5$  dex in oxygen abundances, mainly for the high metallicity regime. These variations can increase even more when higher electron density values, such as the ones found in star-forming clumps (e.g.  $300\text{-}1800 \text{ cm}^{-3}$ , Newman et al. 2012), are considered in abundance determinations.

In this paper, we used long-slit spectroscopic data of a sample of seven pair galaxies to verify the effects of the interaction on the electron density in these systems. This work is organized as follows. In Section 2, we summarize the observations and data reduction. In Section 3, the method to compute the electron density is described. Results and discussion are presented in Sections 4 and 5, respectively. The conclusions of the outcomes are given in Section 6.

## 2 OBSERVATIONS AND DATA REDUCTION

We have selected several systems from Ferreiro & Pastoriza (2004) to study the effects of the kinematics, stellar population, gradient abundances, and electron densities of interacting galaxies. The first results of this programme were presented for AM2306-721 (Krabbe et al. 2008) and AM2322-821 (Krabbe et al. 2011). Table 1 summarizes the main characteristics of the systems: identification, morphology, position, radial velocity, apparent B magnitude, and other designations.

Long-slit spectroscopic data were obtained on May, June, and July 2006 and 2007; and July 2008 with the Gemini Multi-Object Spectrograph (GMOS-S) attached to the 8 m Gemini South telescope, Chile, as part of the poor weather programs GS-2006A-DD-6, GS-2007A-Q-76, and GS-2008A-Q-206. Spectra in the range  $4400\text{-}7300 \text{ \AA}$  were acquired with the B600 grating, and  $1''$  slit width, assuming a compromise between spectral resolution ( $5.5 \text{ \AA}$ ), spectral coverage, and slit losses (due to the Image Quality = ANY constraint). The frames were binned on-chip by 4 and 2 pixels in the spatial and spectra directions, respectively, resulting in a spatial scale of  $0.288'' \text{ px}^{-1}$ , and dispersion of  $0.9 \text{ \AA px}^{-1}$ .

Spectra were taken at different position angles on the sky, with the goal of observing the nucleus and the brightest regions of the galaxies. The exposure time on each single frame was limited to 700 seconds to minimize the effects of cosmic rays, with multiple frames being obtained for each slit position to achieve a suitable signal. The slit positions for each system are shown in Fig. 1, superimposed on the GMOS-S  $r'$  acquisition images. Table 2 gives the journal of observations. Conditions during the observing runs were not photometric, with thin cirrus and image quality in the range  $0.6''$  to  $1.7''$  (as measured from stars in the acquisition images taken just prior to the spectroscopic observations).

The spectroscopic data reduction was carried out using the GEMINI.GMOS package and generic IRAF<sup>1</sup> tasks. We followed the standard procedure: (1) the data were bias subtracted and flat-fielded; (2) the wavelength calibration was established from the Cu-Ar arc frames with typical residuals of  $0.2 \text{ \AA}$  and applied to the object frames; (3) the individual spectra of same slit positions and wavelength range were averaged with cosmic ray rejection; (4) the object frames were sky subtracted interactively using the GSSKYSUB task, which uses a background sample of off-object areas to fit a function to the specified rows, and this fit was then subtracted from the column of each spectra; (5) the spectra were relative flux calibrated using observations of a flux standard star taken with the same set up as the science observations; (6) finally, one-dimensional spectra were extracted from the two-dimensional spectra by summing over four rows along the spatial direction. Each spectrum, therefore, comprises the flux contained in an aperture of  $1'' \times 1.152''$ .

The intensities of the  $\text{H}\beta$ ,  $[\text{O III}]\lambda 5007$ ,  $[\text{O I}]\lambda 6300$ ,  $\text{H}\alpha$ ,  $[\text{N II}]\lambda 6584$ , and  $[\text{S II}]\lambda 6716, \lambda 6731$  emission lines were measured using a single Gaussian line profile fitting on the spectra. We used the IRAF SPLOT routine to fit the lines, with the associated error being given as  $\sigma^2 = \sigma_{cont}^2 + \sigma_{line}^2$ , where

<sup>1</sup> Image Reduction and Analysis Facility, distributed by NOAO, operated by AURA, Inc., under agreement with NSF.

**Table 1.** Galaxy sample.

ID	Morphology	$\alpha(2000)$	$\delta(2000)$	$cz$ (km/s)	$m_B$ (mag)	Others names
AM 1054-325	Sm [2]	10 <sup>h</sup> 56 <sup>m</sup> 58 <sup>s</sup> .2	−33 <sup>h</sup> 09 <sup>m</sup> 52 <sup>s</sup> .0	3 788 [10]	14.55 [2]	ESO 376-IG 027
	Sa [5]	10 57 04.2s	−33 09 21.0	3 850 [5]	15.41 [8]	ESO 376- G 028
AM 1219-430	Sm [6]	12 21 57.3	−43 20 05.0	6 957 [3]	14.30 [7]	ESO 267-IG 041
	S? [6]	12 22 04.0	−43 20 21.0	6 879 [3]	-	FAIRALL 0157
AM 1256-433	E [3]	12 58 50.9	−43 52 30.0	9 215 [3]	14.75 [8]	ESO 269-IG 022 NED01
	E [3]	12 58 50.6	−43 52 53.0	9 183 [3]	16.17 [8]	ESO 269-IG 022 NED02
	SBC [3]	12 58 57.6	−43 50 11.0	9 014 [3]	16.41 [1]	ESO 269-IG 023 NED01
AM 2058-381	Sbc [6]	21 01 39.1	−38 04 59.0	12 383 [3]	14.91 [1]	ESO 341- G 030
	?	21 01 39.9	−38 05 53.0	12 460 [3]	16.24 [1]	ESO 341- G 030 NOTES01
AM 2229-735	SO? [3]	22 33 43.7	−73 40 47.0	17 535 [3]	15.98 [1]	AM 2229-735 NED01
	?	22 33 48.3	−73 40 56.0	17 342 [3]	17.36 [1]	AM 2229-735 NED02
AM 2306-721	SAB(r)c	23 09 39.3	−71 01 34.0	8 919 [4]	14.07 [1]	ESO 077- G 003
	?	23 09 44.5	−72 00 04.0	8 669 [4]	14.47 [1]	ESO 077-IG 004
AM 2322-821	SA(r)c	23 26 27.6	−81 54 42.0	3 680 [3]	13.35 [1]	ESO 012- G 001, NGC 7637
	?	23 25 55.4	−81 52 41.0	3 376 [4]	15.41 [1]	ESO 012- G 001 NOTES01

*References:* [1] Ferreiro & Pastoriza (2004); [2] Weilbacher et al. (2000); [3] Donzelli & Pastoriza (1997); [4] Krabbe et al. (2011); [5] Lauberts (1982)); [6] Paturel et al. (2003); [7] de Vaucouleurs et al. (1991); [8] Lauberts & Valentijn (1989); [9] Huchra et al. (2012); [10] Jones et al. (2009)

*Conventions:*  $\alpha$ ,  $\delta$ : equatorial coordinates

**Table 2.** Journal of observations.

Object	Date	Exposure Time (s)	PA (°)	$\Delta\lambda$ (Å)
AM 1054-325	2007-06-21	4 × 600	77	4280-7130
AM 1219-430	2007-06-06	4 × 600	25	4280-7130
	2007-05-26	4 × 600	162	4280-7130
	2007-06-22	4 × 600	341	4280-7130
AM 1256-433	2007-07-06	4 × 600	292	4280-7130
	2007-06-21	4 × 600	325	4280-7130
AM 2058-381	2006-05-20	4 × 600	42	4351-7213
	2007-05-26	4 × 600	94	4351-7213
	2007-05-24	4 × 600	125	4351-7213
	2007-05-30	4 × 600	350	4351-7213
AM 2229-735	2006-07-20	6 × 600	134	4390-7250
	2006-07-16	6 × 600	161	4390-7250
AM 2306-721	2006-06-20	4 × 600	118	4280-7130
	2006-06-20	4 × 600	190	4280-7130
	2006-06-20	4 × 600	238	4280-7130
AM 2322-821	2006-07-01	3 × 700	59	4280-7130
	2008-07-27	6 × 600	60	4280-7130
	2006-06-30	6 × 600	318	4280-7130

$\sigma_{cont}$  and  $\sigma_{line}$  are the continuum rms and the Poisson error of the line flux, respectively. Furthermore, we considered only measurements whose continuum around  $\lambda$  6700 Å reach a signal-to-noise  $S/N \geq 8$ . The emission line intensities were not corrected for the interstellar extinction, because it is negligible due to the small separation between the [S II] $\lambda$ 6716 and  $\lambda$ 6731 emission lines.

### 3 DETERMINATION OF THE ELECTRON DENSITY

The electron density  $N_e$  was derived from the [S II] $\lambda$ 6716/ $\lambda$ 6731 emission line intensity ratio by solving numerically the equilibrium equation for a  $n$ -level atom approximation using the TEMDEN routine of the NEBULAR package of the STSDAS/IRAF, assuming an electron temperature of 10 000 K, because temperature sensitive emission lines were unobservable in our sample.

The references for the collision strengths, transition probabilities, and energy levels are Ramsbottom et al. (1996), Verner et al. (1987), Keenan et al. (1993), and Bowen et al. (1960). There are two main sources of errors in the determination of electron densities. One is the dependence of the  $N_e$  on the electron temperature  $T_e$  assumed. However, this dependence is weak in the range of temperatures usually found in galactic H II regions (e.g. Copetti et al. 2000). We adopted a mean electron temperature of 10 000 K as a representative value, because it is a typical electron temperature value for these kinds of objects and there are no estimations for our sample. The other main source of error is the saturation of the line ratio for both low and high values of the electron density, which makes the [S II] $\lambda$ 6716/ $\lambda$ 6731 ratio a reliable sensor of the electron density in the range of  $2.45 < \log N_e (\text{cm}^{-3}) < 3.85$  (Stanghellini et al. 1989).

### 4 RESULTS

Fig. 2 shows a sample of the spectra of some H II regions of the galaxies around the [S II] $\lambda$ 6716 and [S II] $\lambda$ 6731 emission lines. The profiles of  $\log([O I]\lambda 6300/H\alpha)$ , [S II] $\lambda$ 6716/ $\lambda$ 6731 ratio, and  $N_e$  as a function of galactocentric radius for the galaxies are shown in Figs. 3-14. The intensity of  $\log([O I]\lambda 6300/H\alpha)$  was plotted only for the apertures for which the electron density determination was possible. The

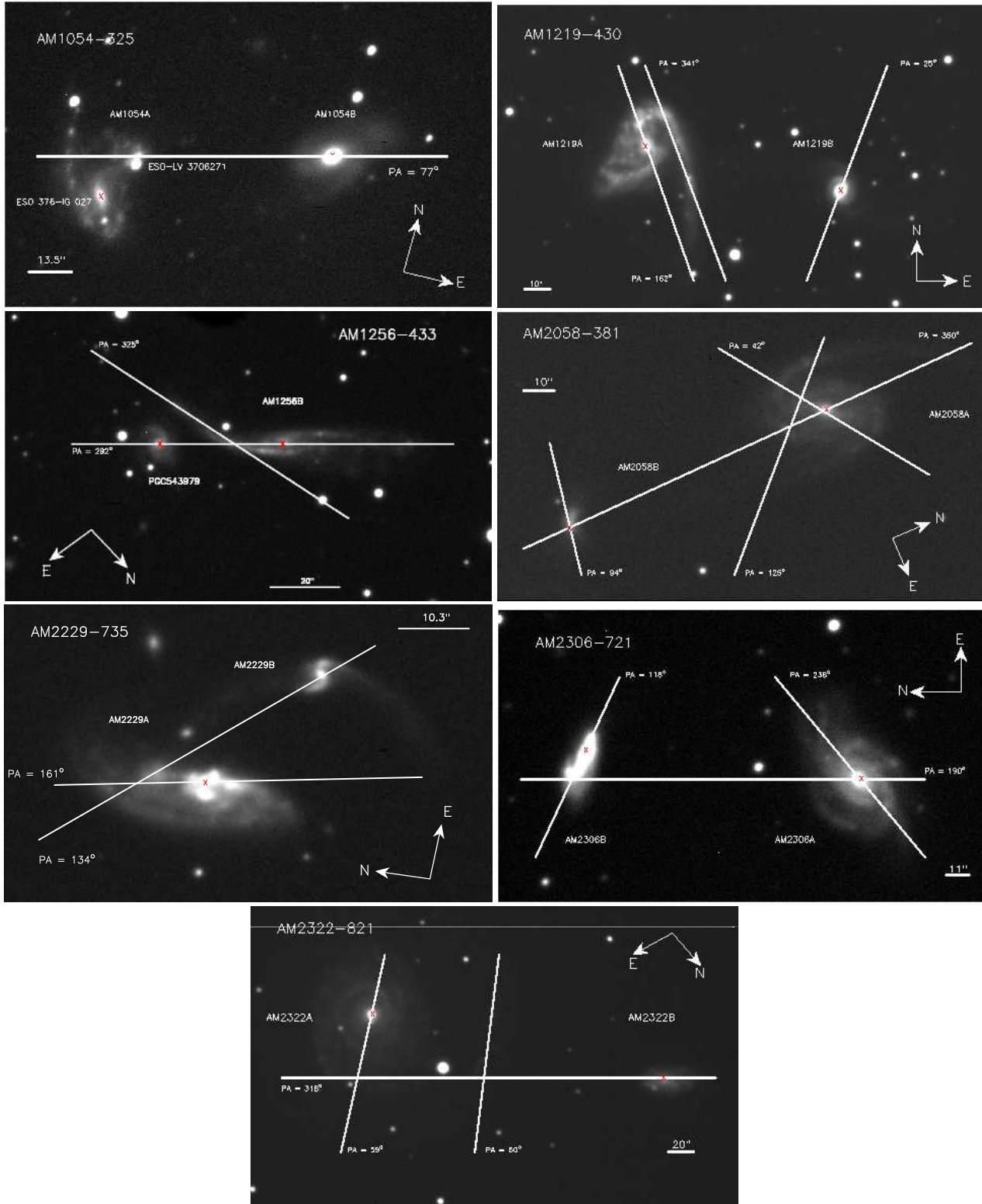


**Figure 1.** The slit positions for each system are shown superimposed on the GMOS-S  $r'$  acquisition image.

galactocentric radius are not corrected by galaxy inclination. In Fig. 1 the adopted centre of each galaxy is marked with a red cross. Table 3 presents some statistics of the  $[\text{S II}] \lambda 6716/\lambda 6731$  ratio and electron density measurements, including the number  $N$  of distinct nebular areas, the mean,

the median, the maximum and minimum, and the standard deviation  $\sigma$ . The results for each system are presented separately.

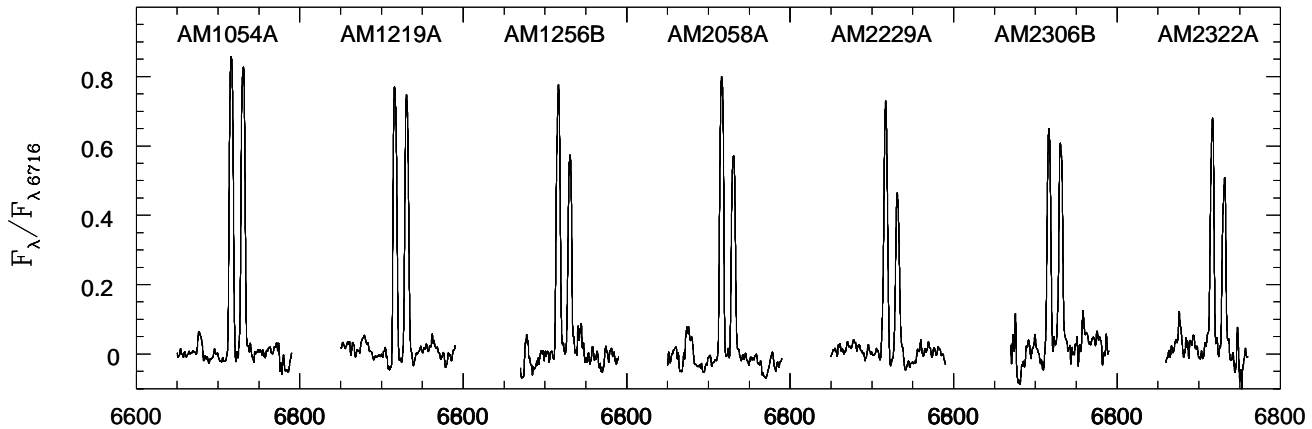


**Figure 2.** A sample of spectra in the range of 6600 to 6800 Å from areas of different galaxies. The flux scale was normalized to the peak of [S II]  $\lambda$  6716.

**Table 3.** [S II] ratio and electron density statistics.

Objects	[S II] $\lambda$ 6716/ $\lambda$ 6731						$N_e$ ( $\text{cm}^{-3}$ )					
	N	mean	median	max	min	$\sigma$	N	mean	median	max	min	$\sigma$
AM 1054A	16	1.19	1.08	1.70	0.97	0.93	13	434	462	681	65	191
AM 1054B	3	0.86	0.85	0.92	0.79	0.07	3	1130	1082	1476	833	324
AM 1219A	29	1.12	1.06	1.77	0.86	0.23	26	532	518	1073	85	286
AM 1219B	5	0.70	0.82	0.92	0.23	0.27	4	1408	1294	2189	855	564
AM 1256B	43	1.48	1.42	2.08	0.99	0.27	22	181	317	626	7	168
AM 2058A	20	1.38	1.26	2.22	0.90	0.37	13	376	318	911	33	263
AM 2058B	8	1.47	1.42	1.80	1.24	0.19	4	86	60	184	42	66
AM 2229A	33	1.60	1.59	2.61	0.19	0.59	7	346	226	686	28	280
AM 2306A	8	1.41	1.44	1.60	1.16	0.16	5	131	107	298	32	99
AM 2306B	15	1.38	1.30	2.88	0.92	0.47	11	300	212	826	19	273
AM 2322A	81	1.41	1.42	1.89	0.85	0.20	41	200	103	1121	11	259
AM 2322B	23	1.47	1.43	1.74	1.35	0.10	12	24	15	75	3	23

#### 4.1 AM 1054-325

This system is composed by a peculiar spiral with disturbed arms (hereafter AM 1054A) and a spiral-like object (hereafter AM 1054B). AM 1054A contains very luminous H II regions along their galactic disk. As can be seen in the Fig. 1, AM 1054A seems to have two nuclei. According to measurements obtained from Weillbacher et al. (2000), the “main” nucleus of this galaxy (ESO 376-IG 027) is the reddest [(B-V)=0.52], while the other (ESO-LV 3760271) has the blue colours of a strong starburst [(B-V)=0.21]. Both nuclei names are marked in the Fig. 1. The measured radial velocity is 3788 km/s (Jones et al. 2009) and 3853 km/s (Sekiguchi & Wolstencroft 1993) for ESO 376-IG 027 and ESO-LV 3760271, respectively. Therefore, the small difference found between their radial velocities together with the perturbed morphology of the galaxy seem to indicate that these objects are gravitationally bound.

For AM 1054A, the electron density values estimated from [S II] $\lambda$  6716/ $\lambda$  6731 ratio (see Fig. 3) present variations of relatively high amplitude along the radius of the galaxy, with the minimum value of  $N_e = 65 \text{ cm}^{-3}$  and the max-

imum of  $N_e = 681 \text{ cm}^{-3}$ . We found a mean density of  $N_e = 434 \pm 53 \text{ cm}^{-3}$ . In this galaxy, the slit position is cutting a bright star-forming region, but does not cross the nucleus of the galaxy. For AM1054B, only few apertures had the [S II] $\lambda$  6716, 6731 emission lines with enough signal to be measured. A mean density of  $N_e = 1130 \pm 187 \text{ cm}^{-3}$  was derived for this galaxy.

#### 4.2 AM 1219-430

This pair is composed by a disturbed spiral (hereafter AM 1219A) and a smaller disk galaxy (AM 1219B). AM 1219A shows a tidal tail produced by the interaction of the galaxies, with very bright H II regions. Systemic velocities of  $6957 \text{ km s}^{-1}$  and  $6879 \text{ km s}^{-1}$  were estimated by Donzelli & Pastoriza (1997) for AM 1219A and AM 1219B, respectively.

The distribution of electron densities exhibits variations of high amplitude across the radius of the main galaxy in the range of  $N_e = 85 - 1073 \text{ cm}^{-3}$ . We found a mean density of  $N_e = 532 \pm 56 \text{ cm}^{-3}$ . As in the case of AM 1054B, only for few apertures of AM 1219B the [S II] $\lambda$  6716, 6731 emission

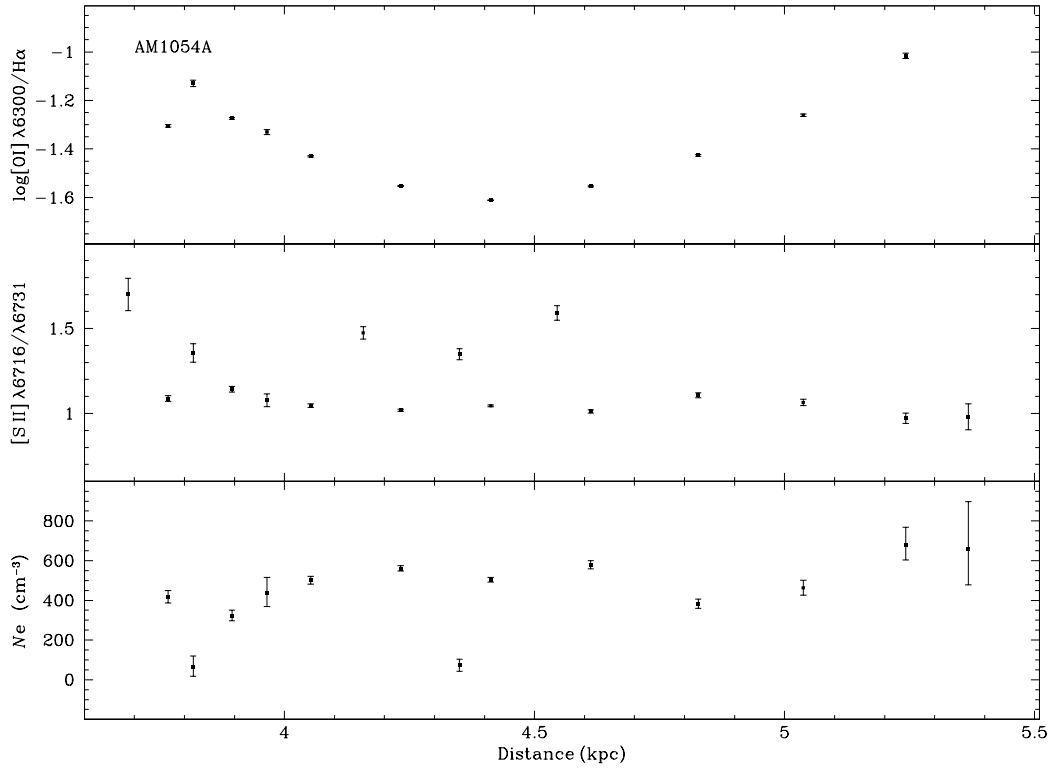


Figure 3. AM 1054-325.  $\log([O I] \lambda 6300/H\alpha)$  ratio,  $[S II] \lambda 6716/\lambda 6731$  ratio, and  $N_e$  as a function of galactocentric radius for AM 1054A.

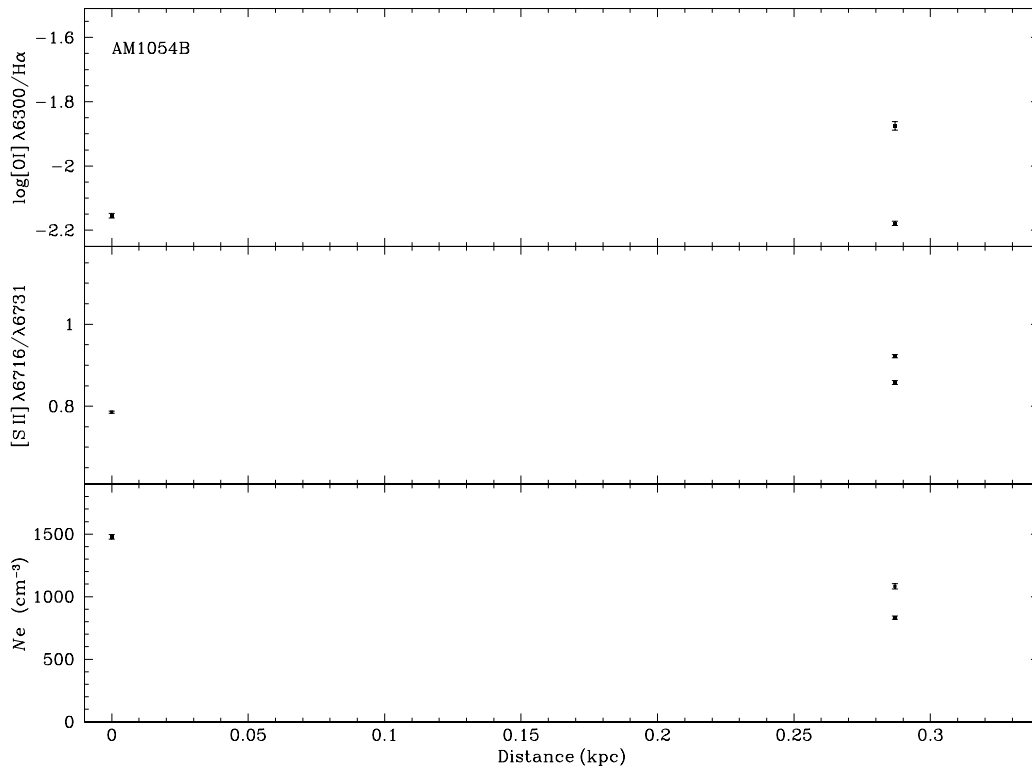


Figure 4. Same as Fig. 3, but for AM 1054B.

lines have enough signal to be measured. A mean density of  $N_e = 1408 \pm 282 \text{ cm}^{-3}$  was derived for this galaxy. Interestingly, the  $N_e$  increases toward the outskirts of this galaxy. This region is at the end of the spiral arm to the Northwest.

#### 4.3 AM 1256-433

AM 1256-433 is a system constituted by three galaxies. Two are elliptical with very bright nuclei, ESO 269-IG 022 NED01 and ESO 269-IG 022 NED02, and one very disturbed spiral galaxy, ESO 269-IG 023 NED01, hereafter AM 1256B. In addition, an isolated disk galaxy, ESO 269-IG 023 NED02/PGC 543979 ( $\alpha = 12^{\text{h}}59^{\text{m}}00^{\text{s}}.6$  and  $\delta = -43^{\text{h}}50^{\text{m}}23^{\text{s}}$  J2000), appears in the field of view of this system, about  $30''$  to the Southeast of the centre of AM 1256B. From our data, we obtained for this isolated galaxy a heliocentric velocity of  $18896 \text{ km s}^{-1}$  indicating that it does not belong to this system, and it was incorrectly associated with AM 1256-433 by Donzelli & Pastoriza (1997); Ferreiro & Pastoriza (2004), and Ferreiro et al. (2008). In Fig. 1, only AM 1256B and the isolated galaxy ESO 269-IG 023 NED02 is shown.

As can be seen in Fig. 7, some regions (for example at about 6 and 12 kpc from the centre of the galaxy) present unphysically large values of the  $[\text{S II}]\lambda 6716/\lambda 6731$  ratio, above the theoretical value of 1.4, the value for the low density limit according to the Osterbrock & Ferland (2006) curve for this relation. There could be some uncertainties associated with the measurements of these sulphur emission lines, due to the placement of the continuum and deblending of the lines, that might produce larger values of the  $[\text{S II}]$  ratio than the expected ones. Values of the  $[\text{S II}]$  ratio larger than the 1.4 upper limit were already observed in other studies using different kinds of instruments (e.g. Kennicutt, Keel, & Blaha 1989; Zaritsky, Kennicutt, & Huchra 1994; Lagos et al. 2009; Relaño et al. 2010; López-Hernández et al. 2013). As pointed out by López-Hernández et al. (2013), the theoretical density determination also needs to be adjusted to the sulphur atomic data and deserves to be revisited. From a spatial distribution study of the electron density in a sample of H II regions in M33, these authors highlighted that when values of the  $\lambda 6716/\lambda 6731$  ratio above the 1.4 limit are obtained, it is reasonable to assume that the electron densities are lower than  $10 \text{ cm}^{-3}$ . They also noted that a safe way to proceed is to take  $N_e = 100 \text{ cm}^{-3}$ , because even before reaching the 1.4 limit, the estimation of the electron density is very uncertain. A mean density of  $N_e = 181 \pm 36 \text{ cm}^{-3}$  was derived for this galaxy. Again, the  $N_e$  increases toward the outskirts of this galaxy, corresponding to the end of the spiral arm at Southeast.

#### 4.4 AM 2058-381

This system of galaxies is a typical M51 type pair. It has a systemic velocity of  $cz = 12286 \text{ km s}^{-1}$  (Donzelli & Pastoriza 1997) and consists of a main galaxy with two spiral arms (hereafter, AM 2058A) and a companion irregular galaxy (hereafter, AM 2058B).

The electron densities obtained for AM 2058A have variations across the galaxy in the range of  $N_e = 33 - 911 \text{ cm}^{-3}$ , and these values are not dependent upon the position.

Due to the small radius of AM 2058B, only a few apertures could be extracted for this galaxy. The electron densities (see Fig. 9) are relatively low, with a mean value of  $N_e = 86 \pm 33 \text{ cm}^{-3}$ , which is compatible with estimations for giant extragalactic H II regions (e.g. Castañeda et al. 1992).

#### 4.5 AM 2229-735

This pair of galaxies consists of a main spiral galaxy strongly disturbed (hereafter AM 2229A) and a smaller disk galaxy that could be connected to the main one by a bridge. AM 2229A has a very massive nucleus of  $M = 5 \times 10^8 M_{\odot}$  (Ferreiro et al. 2008) and very bright H II regions. Only the primary galaxy was observed.

Most of observed regions in AM 2229A present unphysically large values of the S II ratio according to the Osterbrock & Ferland (2006) curve for the relation between this ratio and the electron density. We derived a mean electron density of  $N_e = 346 \pm 95 \text{ cm}^{-3}$ .

#### 4.6 AM 2306-721

AM 2306-721 is a pair composed by a spiral galaxy with disturbed arms (hereafter AM 2306A) interacting with an irregular galaxy (hereafter AM 2306B). Both galaxies contain very luminous H II regions with  $\text{H}\alpha$  luminosity in the range of  $8.30 \times 10^{39} \leq L(\text{H}\alpha) \leq 1.32 \times 10^{42} \text{ erg s}^{-1}$  and high star-formation rate in the range of  $0.07 - 10 M_{\odot} \text{ yr}^{-1}$ , as estimated from  $\text{H}\alpha$  images by Ferreiro et al. (2008).

The few measurements of electron densities provide values in the range of  $N_e = 32 - 298 \text{ cm}^{-3}$  and  $N_e = 19 - 826 \text{ cm}^{-3}$  for AM 2302A and AM 2306B, respectively. Although, we do not have estimates of the electron density at the centre of the main galaxy, the spatial profile seems to indicate an increasing of the  $N_e$  toward the centre of the galaxy, which could be a consequence of gas inflow. Again, in the secondary galaxy, the electron density smoothly increases from about 4 kpc toward the outer regions of the galaxy to the end of the spiral arm at the Southeast.

#### 4.7 AM 2322-821

AM 2322-821 is composed of a SA(r)c galaxy with disturbed arms (hereafter AM 2322A) in interaction with an irregular galaxy (hereafter AM 2322B). Both galaxies contain very luminous H II regions with  $2.53 \times 10^{39} \leq L(\text{H}\alpha) \leq 1.45 \times 10^{41} \text{ erg s}^{-1}$  and star formation rates from 0.02 to  $1.15 M_{\odot} \text{ yr}^{-1}$  (Ferreiro et al. 2008).

The distribution of electron temperatures exhibits variations of very low amplitude across the radius of AM 2322A. One region (at about 2 kpc from the centre of the galaxy) has four values of densities systematically higher than the other apertures along the radius of galaxy. This region is marked in Fig. 15. In this region, the values of densities are in the range of  $N_e = 803 - 1121 \text{ cm}^{-3}$ . We found a mean electron density of  $N_e = 200 \pm 12 \text{ cm}^{-3}$ . AM 2322B presents a relatively homogeneous electron density distribution, with a mean density of  $N_e = 24 \pm 4.8 \text{ cm}^{-3}$ . This is the galaxy with the lowest density in our sample.

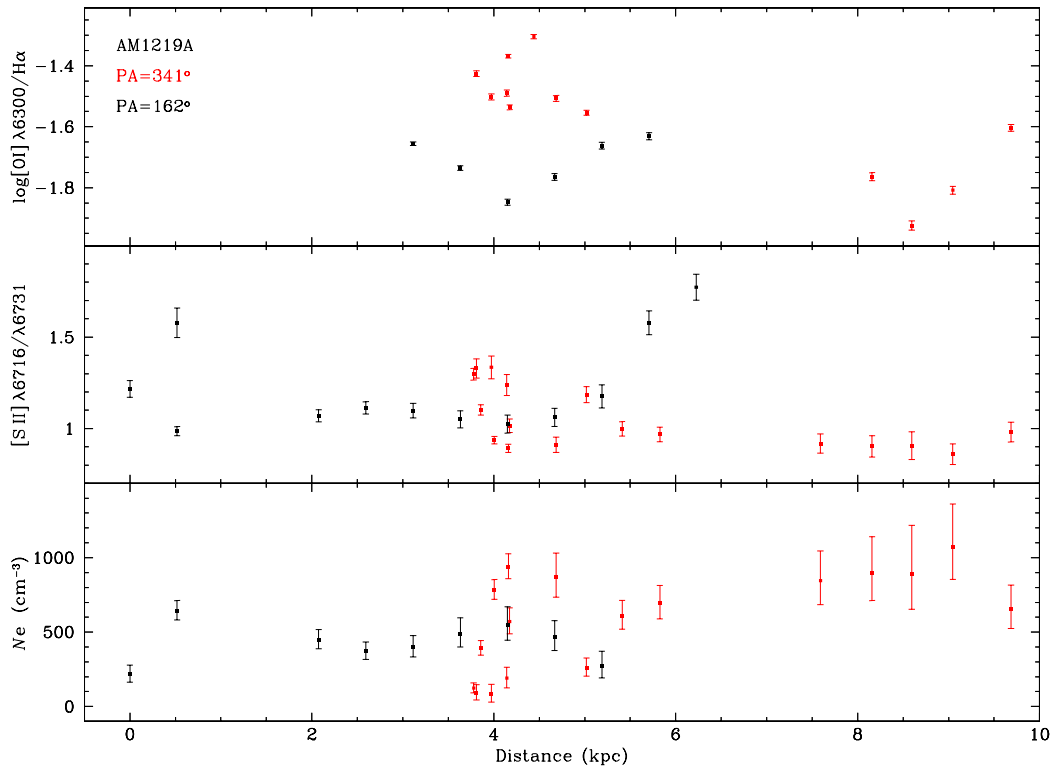


Figure 5. Same as Fig. 3, but for AM 1219A.

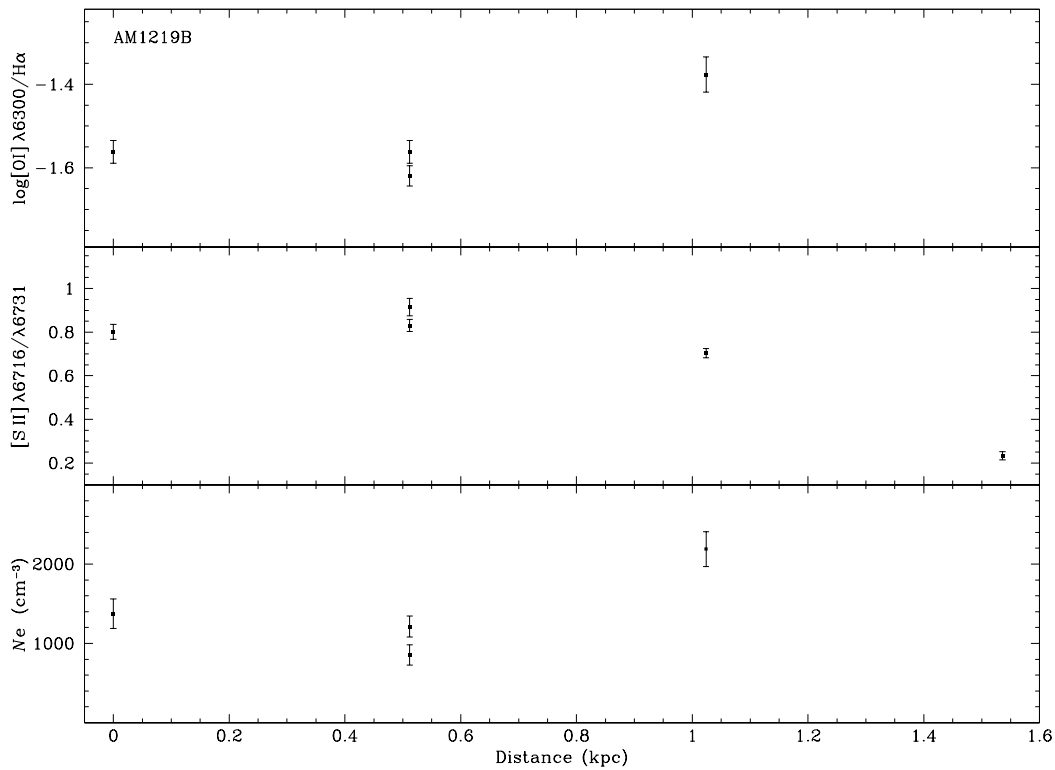


Figure 6. Same as Fig. 3, but for AM 1219B.



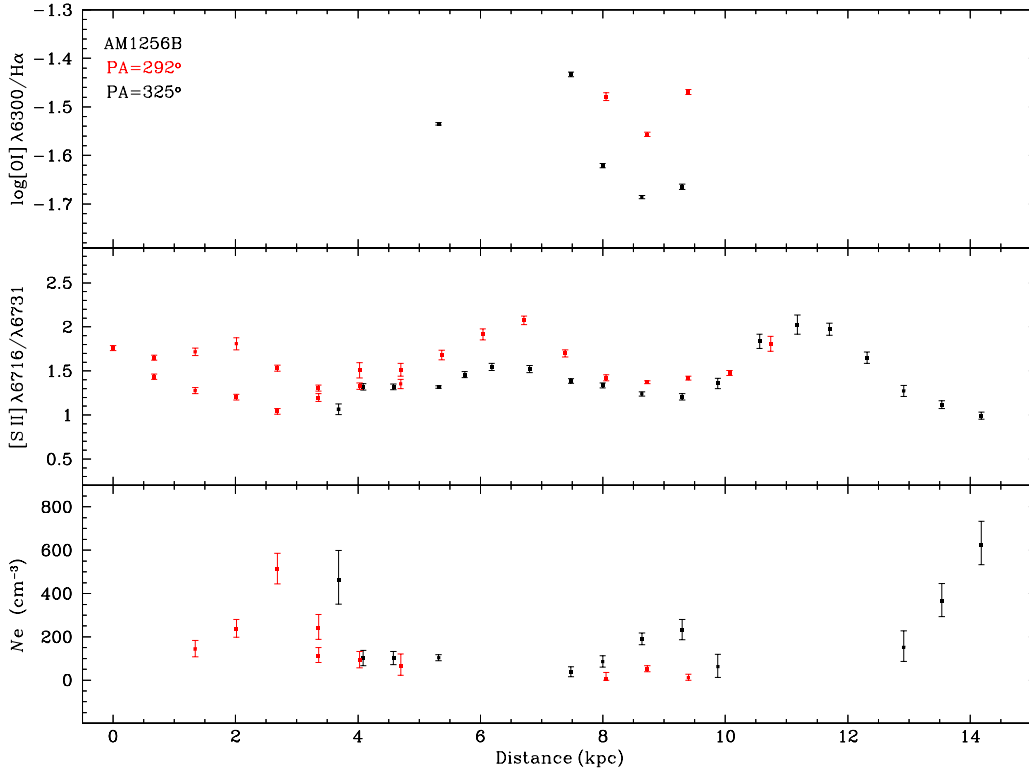


Figure 7. Same as Fig. 3, but for AM1256B.

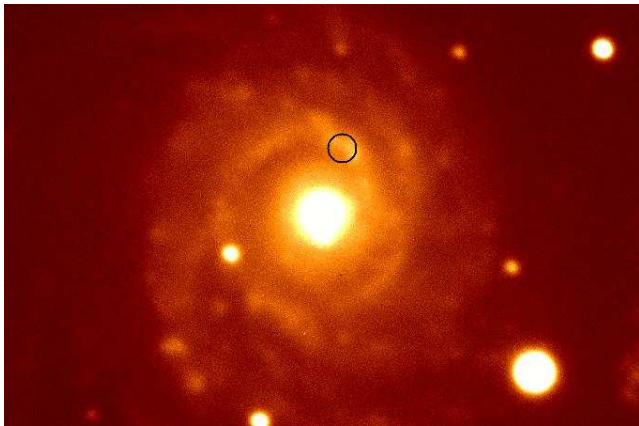


Figure 15. Image of AM2322A with the region of high density (see the text) marked with a circle.

## 5 DISCUSSION

To verify if there are differences between the  $N_e$  values observed in the H II regions of our sample and those obtained in isolated galaxies, we have calculated the electron densities from published measurements of the [S II] line-ratio for disk H II regions in the isolated galaxies M 101, NGC 1232, NGC 1365, NGC 2903, NGC 2997, and NGC 5236 and compared these values with our results. The data of these objects were taken from Kennicutt et al. (2003) for M 101 and from Bresolin et al. (2005) for the other galaxies. The same

atomic parameters and electron temperature adopted for our determinations were used. The spatial profiles of the [S II]  $\lambda 6716/\lambda 6731$  ratio and the electron densities derived for some H II regions in the isolated galaxies are shown in Fig. 16.

As can be seen in this figure, the estimated electron densities are relatively homogeneous along the radius of each isolated galaxy. The derived mean electron densities are in the range of  $N_e = 40 - 137 \text{ cm}^{-3}$ . Only one high value of  $N_e \approx 900 \text{ cm}^{-3}$  is derived in the central region of NGC 5236. It is a metal-rich H II region, with a low electron temperature of  $T_e(\text{O III}) = 4000 \pm 2000 \text{ K}$  and an oxygen abundance of  $12 + \log(\text{O}/\text{H}) \approx 8.9$  dex as derived by Bresolin et al. (2005). This high value can be caused by mass loss and strong stellar winds from embedded Wolf Rayet stars, which are common in metal-rich environments (e.g. Pindao et al. 2002; Bresolin & Kennicutt 2002; Schaerer et al. 2000). If the adopted electron temperature is  $T_e(\text{O III}) = 4000 \text{ K}$ , an estimation of  $N_e \approx 623 \text{ cm}^{-3}$  is obtained. This value is about 30% lower than the one obtained assuming an electron temperature of  $T_e(\text{O III}) = 10000 \text{ K}$ . Then, even though the dependence of the  $N_e$  with the electron temperature is weak, it could have an important effect when temperature fluctuations of high amplitude were observed in H II regions.

The values of the electron density obtained from our sample of interacting galaxies are systematically higher than those derived for the isolated ones. The mean electron density values derived by us for the interacting galaxies in our sample are in the range of  $N_e = 24 - 532 \text{ cm}^{-3}$ ,

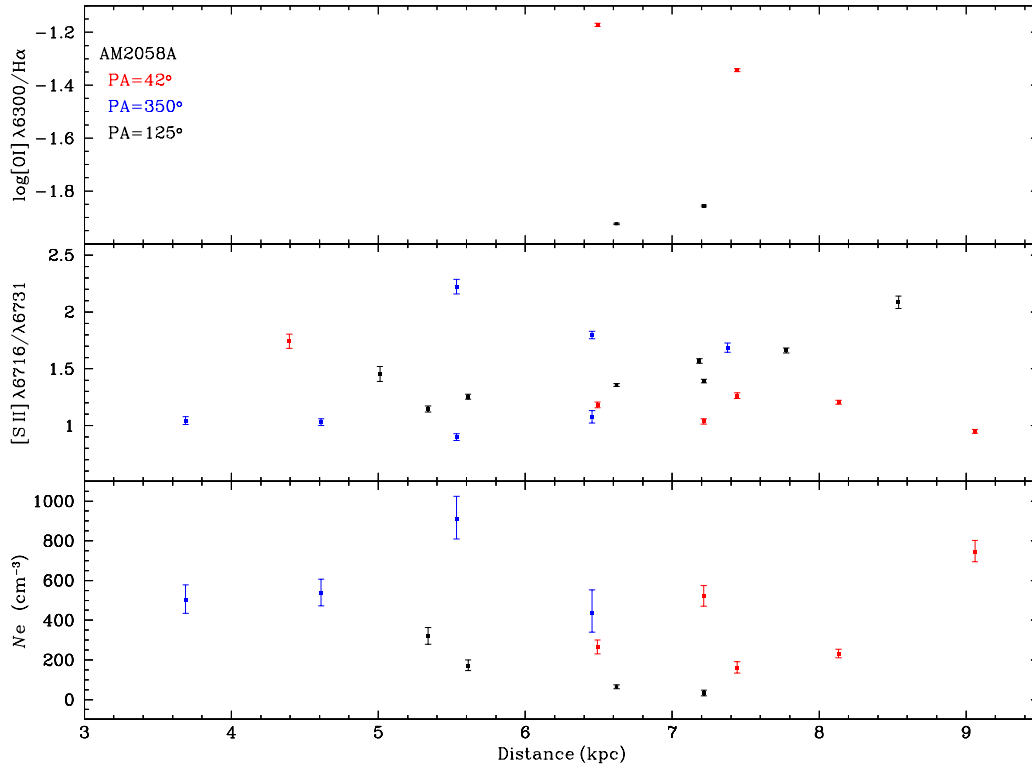


Figure 8. Same as Fig. 3, but for AM 2058A.

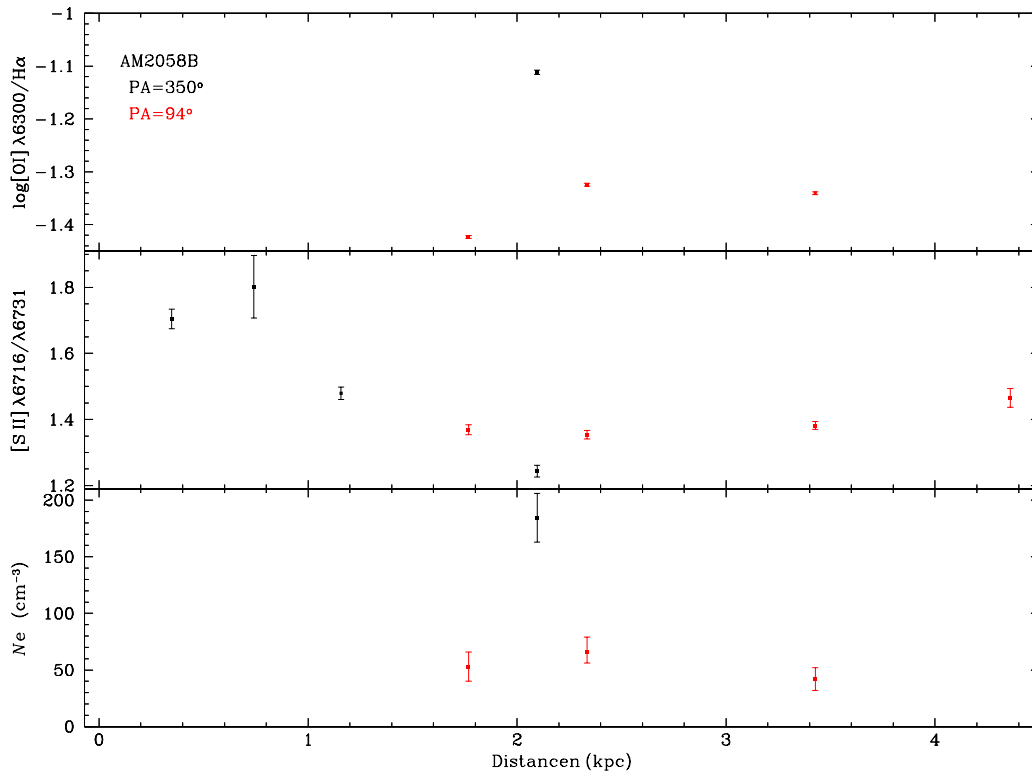


Figure 9. Same as Fig. 3, but for AM 2058B.

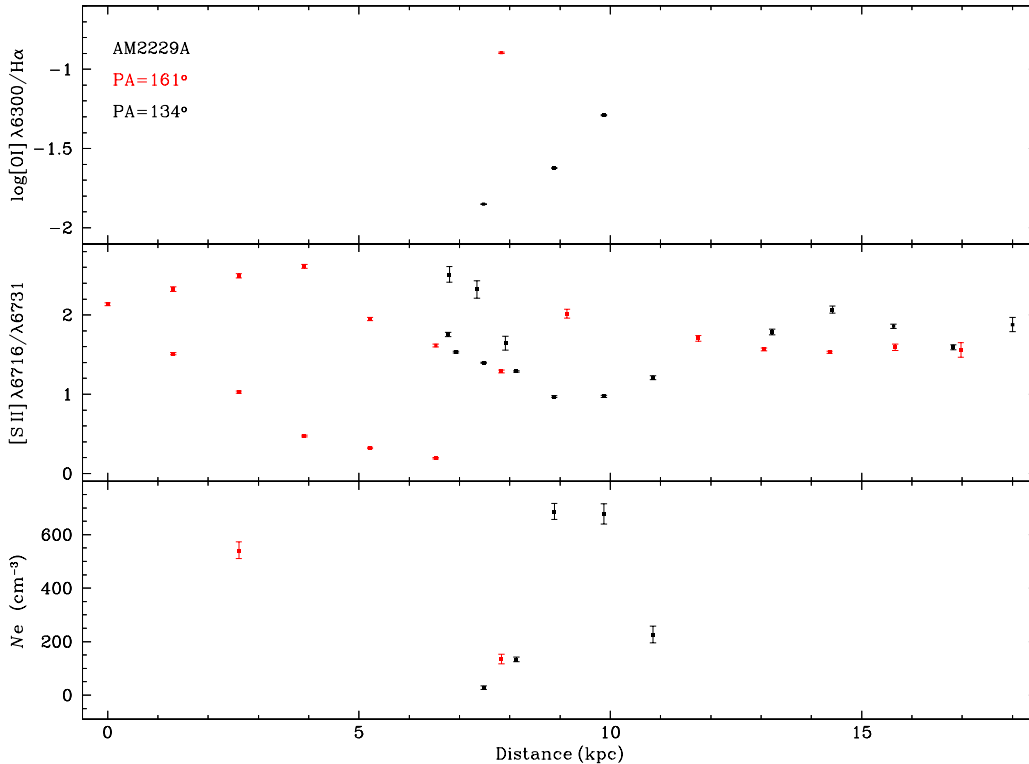


Figure 10. Same as Fig. 3, but for AM 2229A.

which also show higher values than for isolated galaxies. Newman et al. (2012), for the clumpy star-forming galaxy ZC406690, also obtained high electron density values ( $N_e = 300 - 1800 \text{ cm}^{-3}$ ). Moreover, several of our interacting galaxies (AM 2306B, AM 1219A, and AM 1256B) show a slight increment of the  $N_e$  in the outer parts of the galaxy, opposite of what is observed in the isolated galaxies, where the electron density is homogeneous along the radius. The high electron density values found in the outlying parts for the majority of the objects of our sample would be due to zones of induced star formation by direct cloud-cloud interaction (for a review see Bournaud 2011). In these regions, turbulent flows can locally compress the gas, forming over-densities that subsequently cool and collapse into star-forming clouds (Duc et al. 2013; Elmegreen 2002). Although we do not have estimates of the electron density at the centre of AM 2306A, the spatial profile seems to indicate an increasing of  $N_e$  toward the centre of the galaxy, which could be due to inflowing gas. However, in only a few regions in this galaxy were possible to estimate  $N_e$ , therefore, this is a marginal conclusion.

It is worth mentioning that H II regions seemed to be inhomogeneous, and the zones where most of the emission from the ionized gas is originated only occupy a small fraction of the total volume (i.e., small filling factor). Hence, our electron density values derived from the [S II] emission lines are representative of a fraction of the total volume of the H II region (referred as *in situ* electron densities). According to Giammanco et al. (2004), these inhomogeneities, if optically

thick, can modify the determinations of electron temperatures and densities, ionization parameters, and abundances. Copetti et al. (2000) presented a study on internal variation of the electron density in a sample of spatially resolved galactic H II regions of different sizes and evolutionary stages. These authors found that the electron density within H II regions (e.g. S 307) can range from about 30 to  $600 \text{ cm}^{-3}$ , and a filling factor of the order of 0.1 is compatible with their data. Therefore, the estimated electron densities could be about 10% of the *in situ* values sampled by the sulphur line ratio.

An important issue is to study the origin of the high electron density values found in the H II regions of our sample. The presence of gas shock excitation in interacting galaxies is very important not only because they affect quantities derived from spectroscopy, but also due to they act as a mechanism for dissipating the kinetic energy and the angular momentum of the infalling gas in merging systems, as discussed by Rich et al. (2011). The gas shock also increases the density due to the compression of the interstellar material. To analyse if the presence of shock-excited gas produces the high electron density values, the diagnostic diagram  $[\text{O III}]\lambda 5007/\text{H}\beta$  vs.  $[\text{O I}]\lambda 6300/\text{H}\alpha$  proposed by Baldwin et al. (1981) and Veilleux & Osterbrock (1987), and used to separate objects ionized by stars, by shocks and/or active nuclei (AGN) was considered.

In Fig. 17, the diagnostic diagram containing the data of the H II regions studied by us is shown. The galaxy nuclei data are not shown in this diagram. We also show in

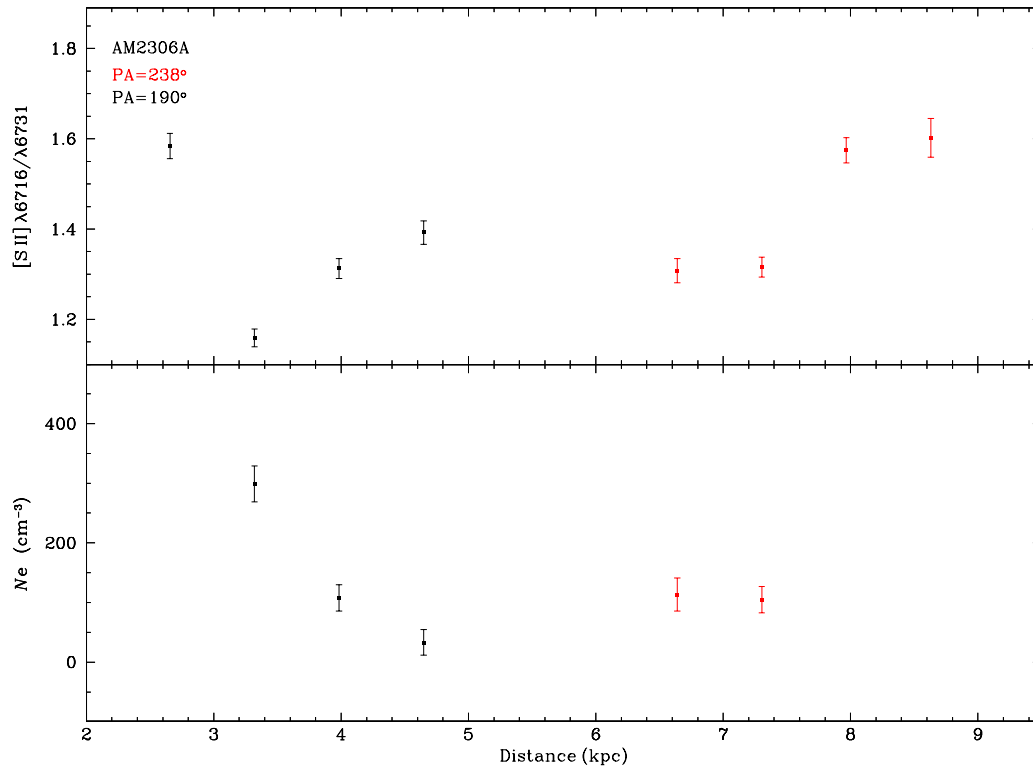


Figure 11. Same as Fig. 3, but for AM 2306A.

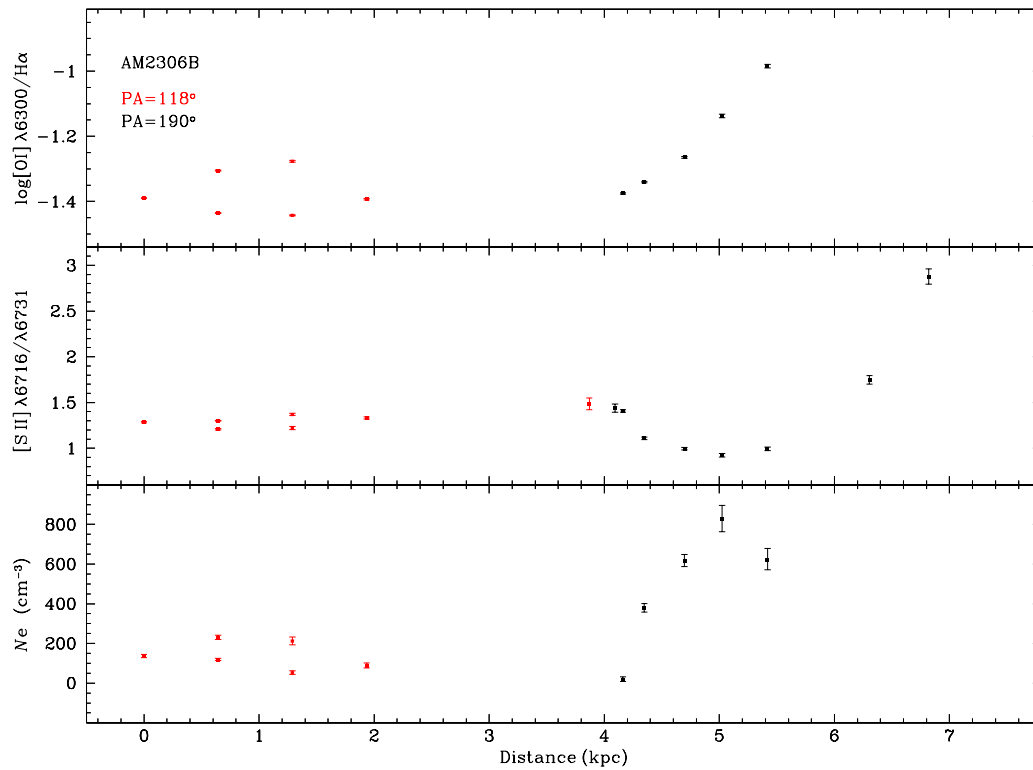


Figure 12. Same as Fig. 3, but for AM 2306B.

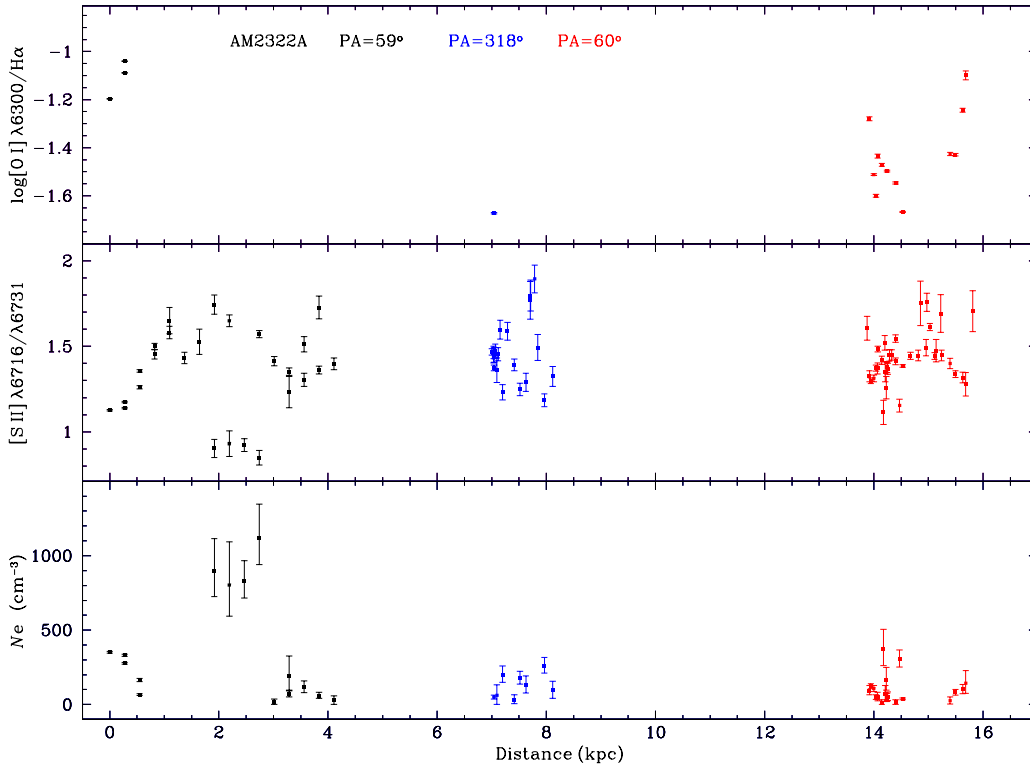


Figure 13. Same as Fig. 3, but for AM 2322A.

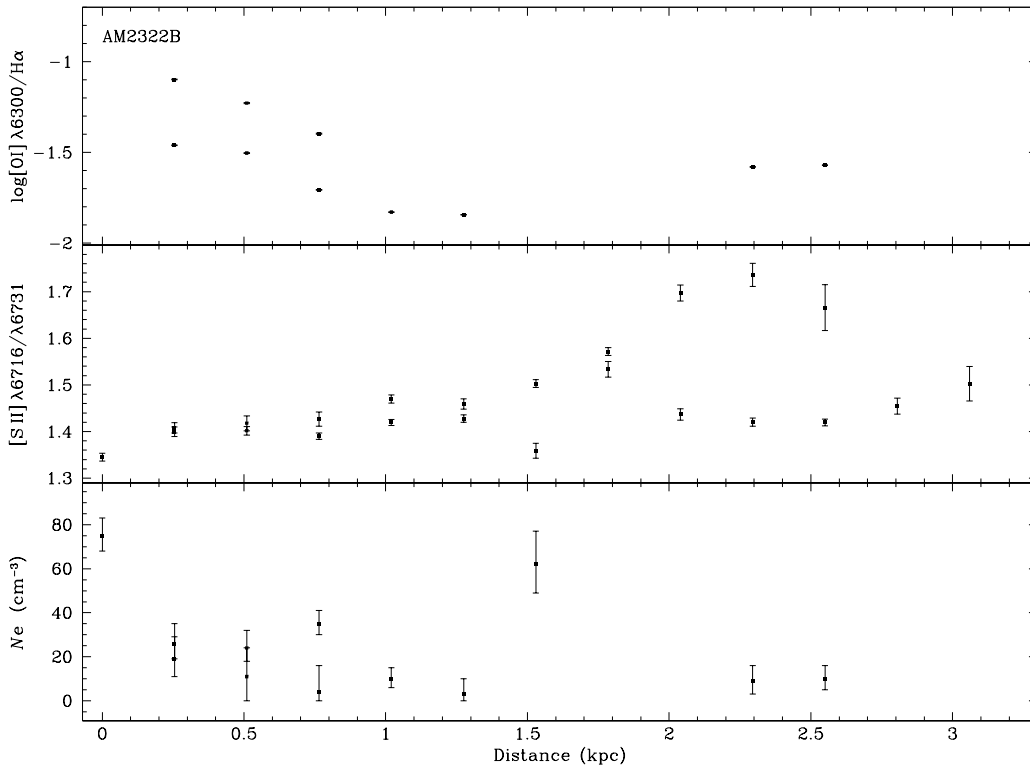
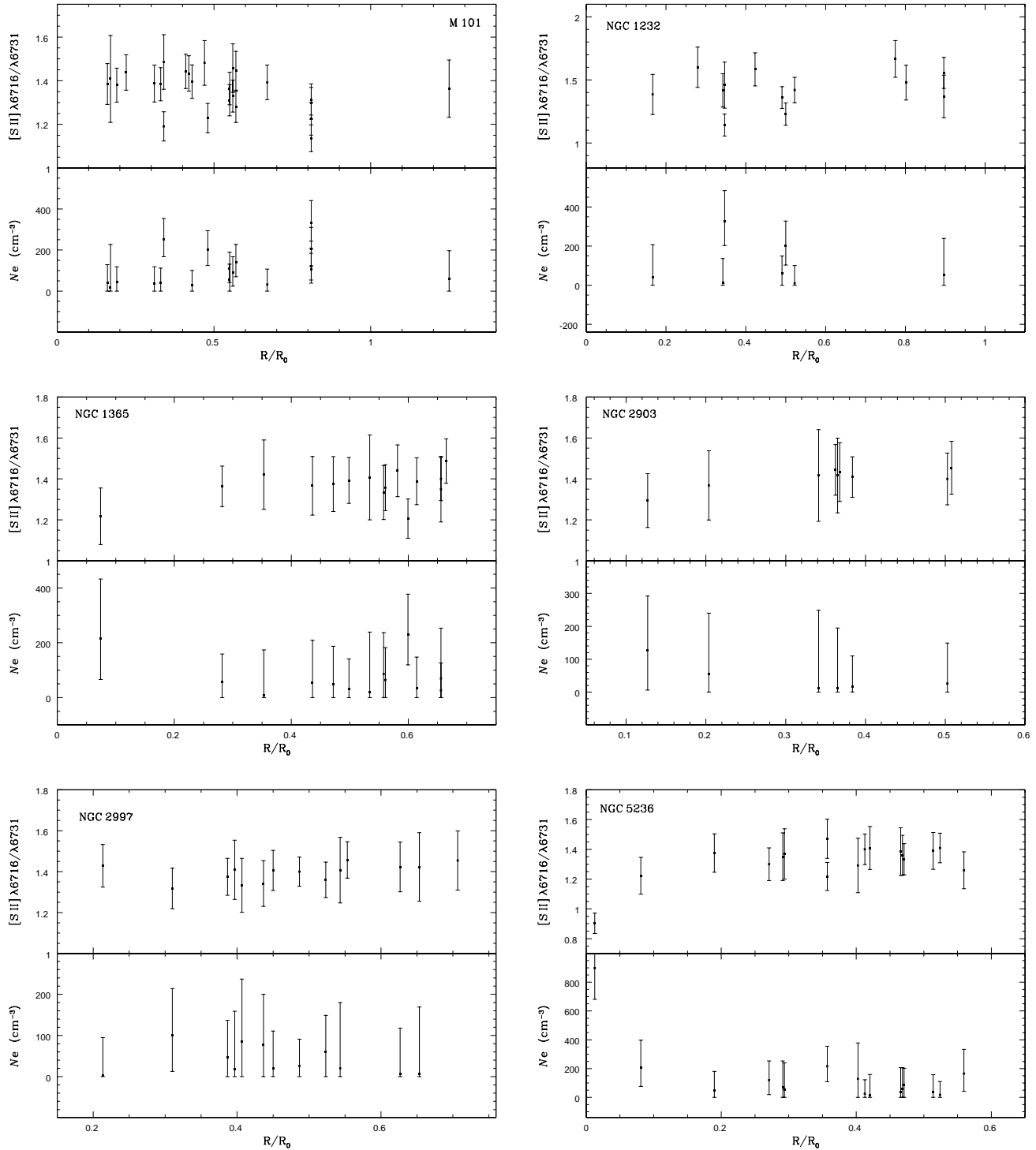


Figure 14. Same as Fig. 3, but for AM 2322B.



**Figure 16.** Profiles of the electron density as a function of  $R/R_0$ , where  $R_0$  is the galactocentric distance deprojected for the isolated galaxies M 101, NGC 1232, NGC 1365, NGC 2903, NGC 2997 and NGC 5236.

this plot, the line proposed by Kewley et al. (2006) to separate objects with distinct ionizing sources: shock gas and massive star excitations. We can see that the all H II regions in AM 1054A, AM 2058B, AM 2306B, and some regions in AM 2322A (3 apertures) and AM 2322B (1 aperture) occupy the area where objects with shock as the main ionizing

source are located. The number of objects represented in Fig. 17 differ from those in the profile figures (Figs. 3-14) because the  $[O III]\lambda 5007/H\beta$  ratio could not be measured for all apertures. From the comparison of the spatial profiles of the electron density and the logarithm of  $[O I]\lambda 6300/H\alpha$  in

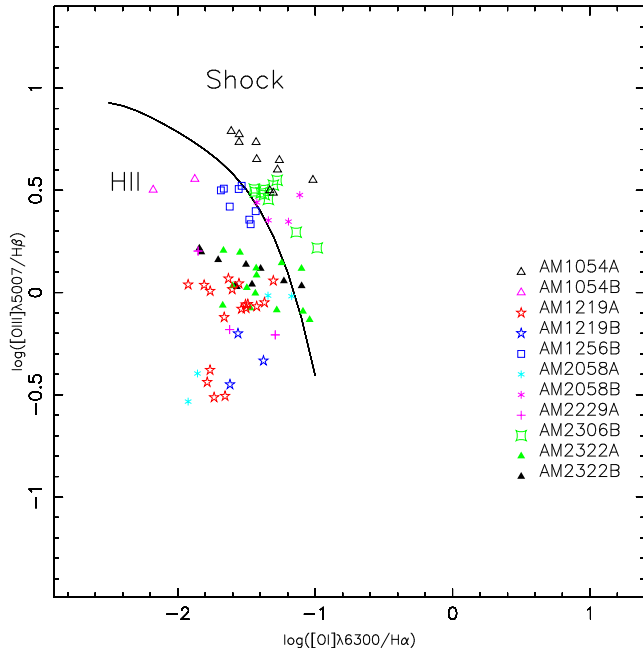


**Figure 17.** Diagnostic diagram of  $[\text{O III}]\lambda 5007/\text{H}\beta$  vs.  $[\text{O I}]\lambda 6300/\text{H}\alpha$ . The black solid line from Kewley et al. (2006) separates the objects ionized by massive stars from the ones containing active nuclei and/or shock excited gas. The data for distinct galaxies are marked by different symbols as indicated. The typical error bar (not shown) of the emission line ratios is about 10 per cent.

the AM 1054A, AM 2058B, and AM 2306B galaxies (Figs. 3, 9 and 12, respectively) we can note the following:

- AM 1054A: All regions of this galaxy have gas shock excitation and the values of electron density are relatively high.
- AM 2058B: It is a small galaxy and only a few apertures could be extracted. As can be seen in Fig. 17, all four disk H II regions of this galaxy have gas shock excitation, and from Fig. 9, we can note that these regions present low electron density values ( $< 200 \text{ cm}^{-3}$ ).
- AM 2306B: the regions with highest  $[\text{O I}]\lambda 6300/\text{H}\alpha$  and  $N_e$  values ( $\approx 700 \text{ cm}^{-3}$ ) lie in the outskirts of galaxy. As can be seen in Fig. 12, it seems to be a trend in this object: from about 4 kpc both the  $N_e$  and the  $[\text{O I}]/\text{H}\alpha$  ratio increase to the outer parts of the galaxy; in the inner part (up to 2 kpc), the profiles of these two quantities are almost flat showing low values.

The cause of the high electron density values associated with the shock excitation region in interacting galaxies is essential to understand how the flux gas works in them. High-velocity gas motions can destroy molecular clouds and quench star formation (Tubbs 1982). To investigate if the high electron density values found in our sample are associated with the presence of excitation by gas shock, we plotted in Fig. 18 the  $N_e$  versus the logarithm of the observed  $[\text{O I}]\lambda 6300/\text{H}\alpha$  emission line ratio. Objects with distinct gas excitation source, in according to Fig. 17, are indicated by different symbols. No correlation is obtained between the presence of shocks and electron densities. The highest elec-

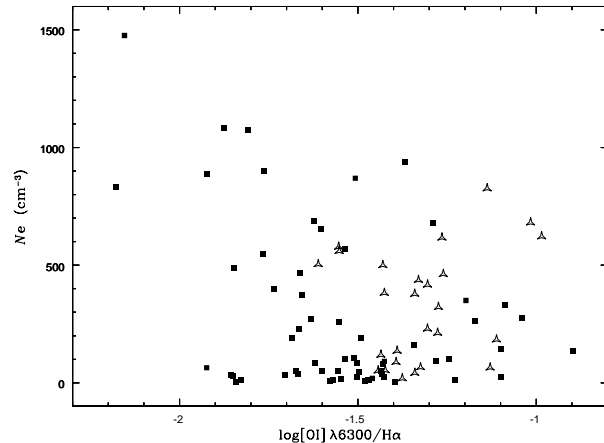


**Figure 18.** Electron density values  $N_e$  derived for our sample versus the observed  $[\text{O I}]\lambda 6300/\text{H}\alpha$  ratio. Squares represent regions ionized by massive stars while triangles represent those with gas shock excitation, according to the diagnostic diagram presented in Fig. 17.

tron density values found in our sample do not belong to objects with gas shock excitation. Therefore, the high electron density values found in the H II regions of our sample do not seem to be caused by the presence of gas shock excitation. However, a deeper analysis such as investigating the presence of correlation between the velocity dispersion of some emission line and its intensity (e.g. Storch-Bergmann et al. 2007) or the implications of multiple kinematical components in the emission line profiles on the derived properties (Hägele et al. 2013, 2012; Amorín et al. 2012) is necessary to confirm our result. Interestingly, the objects with the highest electron density values present the smallest  $[\text{O I}]\lambda 6300/\text{H}\alpha$  line intensity ratios.

## 6 CONCLUSIONS

An observational study of the effects of the interaction on the electron densities from the H II regions along the radius of a sample of interacting galaxies is performed. The data consist of long-slit spectra of high signal-to-noise ratio in the 4390-7250 Å obtained with the Gemini Multi-Object Spectrograph at Gemini South (GMOS). The electron density was determined using the ratio of lines  $[\text{S II}]\lambda 6716/\lambda 6731$ . The main findings are the following:

- The electron density estimates obtained for some H II regions of our sample of interacting galaxies are systematically higher than those derived for isolated galaxies in the literature. The mean electron density values of interacting galaxies are in the range of  $N_e = 24 - 532 \text{ cm}^{-3}$ , while those obtained for isolated galaxies are in the range of  $N_e = 40 - 137 \text{ cm}^{-3}$ .
- Some interacting galaxies: AM 2306B, AM 1219A, and AM 1256B show an increment of  $N_e$  toward the outskirts of each system. This kind of relation is not observed in isolated galaxies, where the electron density profile is rather flat along the radius of each galaxy.
- The galaxies where the mechanism of gas shock excitation is present in almost all the H II regions are AM 1054A,

AM 2058B, and AM 2306B. For the remaining galaxies, only few H II regions has emission lines excited by shocks, such as in AM 2322B (1 point) and AM 2322A (4 points). It is noteworthy that only in three of all objects analysed here the main excitation mechanism for all of their H II regions is shocks.

- No correlation is obtained between the presence of shocks and electron densities. Indeed, the highest electron density values found in our sample do not belong to the objects with gas shock excitation. Therefore, the high electron density values found in the H II regions of our sample do not seem to be caused by the presence of gas shock excitation.

## ACKNOWLEDGEMENTS

Based on observations obtained at the Gemini Observatory, which is operated by the Association of Universities for Research in Astronomy, Inc., under a cooperative agreement with the NSF on behalf of the Gemini partnership: the National Science Foundation (United States), the Science and Technology Facilities Council (United Kingdom), the National Research Council (Canada), CONICYT (Chile), the Australian Research Council (Australia), Ministério da Ciência e Tecnologia (Brazil), and SECYT (Argentina).

A. C. Krabbe, O. L. Dors Jr., and D. A. Rosa thank the support of FAPESP, process 2010/01490-3, 2009/14787-7, and 2011/08202-6 respectively.

We also thank Ms. Alene Alder-Rangel for editing the English in this manuscript.

## REFERENCES

- Allen, M., Brent, A., Dopita, M. A. 2008, *ApJS*, 178, 20
- Amorín R., Vílchez J. M., Hägele G. F., Firpo V., Pérez-Montero E., Papaderos P., 2012, *ApJ*, 754, L22
- Baldwin, J. A., Phillips, M. M., Terlevich, R. 1981, *PASP*, 93, 5
- Bournaud, F. 2011, *EAS Publications Series*, 51, 107
- Bowen, I. S., 1960, *ApJ*, 132, 1.
- Bresolin, F., Schaerer, D., González Delgado, R. M., Stasińska, G. 2005, *A&A*, 441, 981
- Bresolin, F., & Kennicutt, R. C. 2002, *ApJ*, 572, 838
- Castañeda, H. O., Vílchez, J. M., Copetti, M. V. F. 1992, *A&A*, 260, 370
- Copetti, M. V. F., Mallmann, J. A. H., Schmidt, A. A.; Castañeda, H. O. 2000, *A&A*, 357, 621
- Copetti, M. V. F., & Writzl, B. C. 2002, *A&A*, 382, 282
- de Vaucouleurs, G., de Vaucouleurs, A., Corwin, H. G., Jr., et al. 1991, *Book-Review - Third Reference Catalogue of Bright Galaxies Sky and Telescope*, 82, 621
- Donzelli, C. J., Pastoriza, M. G. 2000, *AJ*, 120, 189
- Donzelli, C. J., Pastoriza, M. G. 1997, *ApJS*, 111, 181
- Dopita, M. A., Kewley, L. J., Heisler, C. A., Sutherland, R. S. 2000, *ApJ*, 542, 224
- Dors J. O. L., Krabbe A., Hägele G. F., Pérez-Montero E., 2011, *MNRAS*, 415, 3616
- Dors, O. L., Storchi-Bergmann, T., Riffel, R. A., Schimdt, A. A. 2008, *A&A*, 482, 59
- Duc, P.-A., Belles, P.-E., Brinks, E., Bournaud, F. 2013, *Proceedings of the International Astronomical Union*, 292, 323
- Elmegreen, B. G. 2002, *ApJ*, 577, 206
- Ferreiro, D. L., Pastoriza, M. G. 2004, *A&A*, 428, 837
- Ferreiro, D. L., Pastoriza, M. G., Ricketts, M. 2008, *A&A*, 481, 645
- Giammanco, C., Beckman, J. E., Zurita, A., & Relaño, M. 2004, *A&A*, 424, 877
- Hägele G. F., Firpo V., Bosch G., Díaz Á. I., Morrell N., 2012, *MNRAS*, 422, 3475
- Hägele G. F., Díaz Á. I., Terlevich R., Terlevich E., Bosch G. L., Cardaci M. V., 2013, *MNRAS*, 432, 810
- Huchra, J. P., Macri, L. M., Masters, K. L., et al. 2012, *ApJS*, 199, 26
- Jones, D. H., Read, M. A., Saunders, W., et al. 2009, *MNRAS*, 399, 683
- Keenan, F. P. and Hibbert, A. and Ojha, P. C. and Collon, E. S. 1993, *Phys. Scr. A.*, 47, 48-129.
- Kennicutt, R. C., Bresolin, F., Garnett, D. R. 2003, *ApJ*, 591, 801
- Kennicutt R. C., Jr., Keel W. C., Blaha C. A., 1989, *AJ*, 97, 1022
- Kennicutt, R. C. 1984, *ApJ*, 287, 116
- Kewley, L. J., Groves, B., Kauffmann, G., & Heckman, T. 2006, *MNRAS*, 372, 961
- Kewley L. J., Rupke D., Jabran Hahid H., Geller M. J., Barton E. J., 2010, *ApJ*, 721, L48
- Kewley L. J., & Dopita, M. A. 2002, *ApJSS*, 145, 35
- Krabbe, A. C., Pastoriza, M. G., Winge, Cláudia, Rodrigues, I., Dors, O. L., Ferreiro, D. L. 2011, *MNRAS*, 416, 38
- Krabbe, A. C.; Pastoriza, M. G.; Winge, Cludia; Rodrigues, I.; Ferreiro, D. L.
- Lauberts, A., & Valentijn, E. A. 1989, *The Messenger*, 56, 31
- Lauberts, A. 1982, *Garching: European Southern Observatory (ESO)*, 1982,
- Lagos P., Telles E., Muñoz-Tuñón C., Carrasco E. R., Cuisinier F., Tenorio-Tagle G., 2009, *AJ*, 137, 5068
- López-Hernández J., Terlevich E., Terlevich R., Rosa-González D., Díaz Á., García-Benito R., Vílchez J., Hägele G., 2013, *MNRAS*, 430, 472
- Martin, P., & Roy, J.-R. 1995, *ApJ*, 445, 161
- Newman, S. F., Shapiro Griffin, K., Genzel, R. et al. 2012, *ApJ*, 752, 111
- O'Dell, C. R., & Castañeda, H. O. 1984, *ApJ*, 283, 158
- Oey, M. S., & Kennicutt, R.C. 1993, *ApJ*, 411, 137
- Osterbrock D. E., Ferland G. J., 2006, *agna.book*,
- Patrel G., Petit C., Prugniel P., Theureau G., Rousseau J., Brouty M., Dubois P., Cambrésy L., 2003, *A&A*, 412, 45
- Puech, M., Flores, H., Hammer, F., Lehnert, M. D., 2006, *A&A*, 455, 131,134.
- Pindao, M., Schaerer, D., González Delgado, R. M., Stasińska, G. 2002, *A&A*, 394, 443
- Ramsbottom, C. A. and Bell, K. L. and Stafford, R. P. 1996, *Atomic Data and Nuclear Data Tables*, 63, 57.
- Relaño M., Monreal-Ibero A., Vílchez J. M., Kennicutt R. C., 2010, *MNRAS*, 402, 1635
- Rupke D. S. N., Kewley, L. J., Chien, L.-H 2010, *ApJ*, 710, L156
- Rich, J. A., Kelley, L. J., Dopita, M. A. 2011, *ApJ*, 734, 87



- Rich, J. A., Torrey, T., Kelley, L. J., Dopita, M. A., Rupke, D. S. N. 2012, ApJ, 753, 5
- Schaerer, D., Guseva, N. G., Izotov, Y. I., Thuan, T. X. 2000, A&A, 362, 53
- Sekiguchi, K., & Wolstencroft, R. D. 1993, MNRAS, 263, 349
- Stanghellini, L., & Kaler, J. B. 1989, ApJ, 343, 811
- Soto, K. T., Martin, C. L. 2012, ApJS, 203, 3
- Soto, K. T., Martin, C. L., Prescott, M. K. M., Armus, L. 2012, ApJS, 757, 86
- Scudder, J. M., Ellison, S. L., Torrey, P., Patton, D. R., Trevor Mendel, J. 2012, astro-ph/1207.479
- Storchi-Bergmann, T., Dors, O. L., Riffel, R. A. et al. 2007, ApJ, 670, 959
- Tubbs, A. D. 1982, ApJ, 255, 458
- Verner, D. A. and Verner, E. M. and Ferland, G. J. 1987, Atomic Data and Nuclear Data Tables, 1, 64.
- Veilleux, S., Cecil, G., Bland-Hawthorn, J. 2005, ARA&A, 43, 76
- Veilleux, S., & Osterbrock, D. E. 1987, ApJS, 63, 295
- Weilbacher, P. M., Duc, P.-A., Fricke, K. J., Alvensleben, U., Martin, P., & Fricke, K. J. 2000, A&A, 358, 819
- Zaritsky D., Kennicutt R. C., Jr., Huchra J. P., 1994, ApJ, 420, 87